Journal of Magnetism and Magnetic Materials 568 (2023) 170349

Contents lists available at ScienceDirect

Journal of Magnetism and Magnetic Materials

journal homepage: www.elsevier.com/locate/jmmm

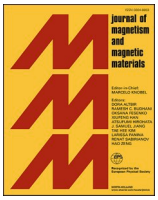

Decoupling the effects of texture and composition on magnetic properties of Fe-Si sheet processed by shear deformation

Andrew B. Kustas [a,*], James B. Mann [e], Kevin P. Trumble [b,d], Srinivasan Chandrasekar [c,d]

[a] Material, Physical, and Chemical Sciences Center, Sandia National Laboratories, Albuquerque, NM 87185, United States
[b] School of Materials Engineering, Purdue University, West Lafayette, IN 47907, United States
[c] School of Industrial Engineering, Purdue University, West Lafayette, IN 47907, United States
[d] Center for Materials Processing and Tribology, Purdue University, West Lafayette, IN 47907, United States
[e] M4 Sciences Corporation, Lafayette, IN 47906, United States

ARTICLE INFO

Keywords:
Magnetic materials
Electrical steel
Severe plastic deformation
Crystallographic texture
Magnetic properties
Sheet processing

ABSTRACT

Soft magnetic Fe-Si alloys (electrical steels) possess exceptional functional properties such as high permeability, low coercivity, and low core loss, which generally improve with increasing Si content in the alloy. However, Fe-Si alloys containing > 3.5 wt% Si are also characterized by prohibitively low workability and poor ductility that have prevented their efficient commercial production in sheet form by rolling. This has limited their use for improving efficiency of motors and transformers. In this study, hybrid cutting-extrusion (HCE) is used as a single-step thermomechanical processing method to produce continuous Fe-Si alloy sheet with high Si compositions of 4 wt% to 6.5 wt%. HCE sheet is shown to have a homogeneous annealed grain structure and simple-shear crystallographic textures. By controlling the HCE deformation path, varied crystallographic shear textures are created in the sheet. Quasi-static magnetic properties of the HCE sheet are evaluated to decouple the effects of sheet texture and Si composition on resultant permeability and coercivity properties. The results suggest that HCE, with suitable process scaling, is a viable route for production of high-Si content electrical steel sheet for next-generation motors and transformers.

1. Introduction

Iron-silicon (Fe-Si) alloy sheet possesses favorable electric and magnetic properties for motor and transformer cores, including high electrical resistivity, high magnetic permeability (μ), high saturation induction (B_s), low coercivity (H_c) and low core loss. These properties are controlled by the material composition and microstructure, principally the grain size [1], crystallographic texture [2], and Si content [3]. Commercial processing of Fe-Si sheet, using multiple steps of hot and cold rolling (10–20 steps), with intermediate annealing stages, has been successful in producing two types of sheet products, the so-called grain oriented and non-grain oriented sheet. These two types of sheet materials having distinctly different microstructures and magnetic properties [4,5]. While rolled Fe-Si sheet is paramount to a variety of electromagnetic devices, the commercial rolling processes that are used to produce them have significant limitations. The limitations include restricted control of sheet crystallographic texture, and difficulty/inability to process Fe-Si alloys with high silicon content > 3.5 wt% Si due to their poor workability. Overcoming these limitations, especially the latter to enable the ideal 6.5 wt% Si composition from a magnetic properties perspective, is important for developing next generation electromagnetic devices (e.g., motors, transformers) with higher efficiencies and reduced core loss [6]. While previous research has demonstrated alternative methods for producing Fe-Si sheet with higher Si contents near 6.5 wt%, such as casting [7,8], sputter deposition [9], spray forming [10], direct powder rolling [11] and CVD siliconizing [12], only the CVD process has led to commercial products. But the use of the CVD siliconized steels is restricted by their high cost driven by high processing temperatures and times required for sufficient diffusion of Si throughout the sheet thickness. Furthermore, none of these processing methods has enabled widespread commercial replacement of the conventional (rolled) Fe-1 to 3.5 wt% Si sheet currently in use, despite the inherently improved properties predicted at higher Si contents.

Recently, a promising thermomechanical processing alternative to rolling was shown to enable production of Fe-Si alloy sheet with Si contents up to 6.5 wt% Si, a range of grain sizes, and crystallographic

* Corresponding author.
E-mail address: akustas@sandia.gov (A.B. Kustas).

https://doi.org/10.1016/j.jmmm.2022.170349
Received 18 August 2022; Received in revised form 8 December 2022; Accepted 30 December 2022
Available online 3 January 2023

textures [13,14]. The process is hybrid cutting-extrusion (HCE), wherein sheet is peeled off from ingot by confined shear deformation in a single step, reminiscent of cutting. By varying the deformation path, a range of shear (crystallographic) textures is enabled in the sheet by the HCE – textures difficult, if not impossible, to achieve by rolling.

In this study, we present detailed magnetic properties characterization of Fe-Si sheet, of high Si content, produced by the HCE. The control of deformation afforded by the processing route allows for the effects of crystallographic texture, grain size and Si content on magnetic properties to be decoupled; and production of sheet material from low-workability, high-Si content Fe alloys. The results show that the magnetic properties are relatively insensitive to the crystallographic texture orientation, perhaps even more so than the commercial non-grain oriented electrical steel sheet [15], with only minor changes in coercivity and permeability recorded. Softer magnetic properties are obtained in sheet with higher (6.5 %) Si content - an increase in maximum permeability of ~ 180 % and a decrease in coercivity of ~ 240 %. Implications of the results for deformation processing of high-Si electrical steels into sheet forms are briefly discussed.

2. Experimental procedures and details

A concise summary of the HCE process is given below, with more details of the process mechanics to be found elsewhere [16]. Fig. 1 shows a rotary configuration of the HCE used to produce sheet. The process utilizes a sharp, wedge-shaped cutting tool (primary tool) and a second constraint tool/die, located directly across from the primary tool, to simultaneously cut and extrude sheet/strip of predefined thickness t_o from a rotating cylindrical workpiece (WP) material. The peeled extrudate (sheet) is created by large-strain deformation in simple shear imposed along a narrow deformation zone often idealized as a plane OA, see Fig. 1. The sheet is thus formed in a single deformation step to a final thickness t_c, either from an initial cast or wrought ingot, by constrained chip-formation. The highly-confined shear deformation promotes adiabatic heating, while the HCE deformation geometry imposes large hydrostatic pressure (~hardness) in the deformation zone, both of which enhance material workability. This workability enhancement, observed earlier in HCE of hcp metals [16,17] and unique in the context of thermomechanical processing, also enables continuous sheet from low-workability bcc Fe-Si alloys, including the 4 wt% and 6.5 wt% Si systems, to be produced whereas rolling is unsuccessful (Fig. 1c) [14].

The deformation in the sheet is controlled by the tool rake angle α and the distance between the cutting and constraint tools, defined by the chip thickness ratio $\lambda = t_c/t_o$. The deformation strain and strain path, influencing sheet grain size and crystallographic texture, are determined by the HCE parameters. The deformation strain ε (scalar von Mises effective strain) can be estimated for the idealized shear plane deformation by:

$$\varepsilon = \frac{1}{\sqrt{3}}\left(\frac{\lambda}{\cos\alpha} + \frac{1}{\lambda\cos\alpha} - 2\tan\alpha\right) \quad (1)$$

For a given cutting tool rake angle, α, this strain is a minimum for $\lambda = 1$. It increases steeply with increasing/decreasing λ on either side of this minimum. Large effective strains ($\varepsilon > 1$) can be imposed by the shear-based deformation process to effect grain refinement and produce sheet with ultrafine grained microstructures. In the present study, the sheet strain is kept constant at ~ 1.25. The sheet is annealed prior to the magnetic properties characterization, so as to remove any influences due to grain size and imposed strain on the magnetic properties [13,18].

The orientation of the deformation zone OA in Fig. 1, which is controlled by the strain path, determines the sheet crystallographic texture. Using the rake face normal (RFN) and chip flow directions (CFD) as reference axes (see Fig. 1b), the deformation zone orientation with respect to the sheet surface, i.e. shear plane angle, can be used to predict the sheet texture. This is given by:

$$\phi' = 90^\circ + \alpha - \phi \quad (2)$$

where ϕ is equal to $\tan^{-1}(\cos\alpha/(\lambda - \sin\alpha))$. This predicted orientation or shear plane angle can be compared with the measured texture orientation (equivalent ϕ') to see how effective the strain path is, as a signature of deformation texture.

Direct *in situ* measurement of the strain rate and strain fields using high-speed imaging of the deformation have shown that ϕ' provides an accurate first-order characterization of the HCE strain path and resultant crystallographic texture in the sheet [17,19]. Crystallographic shear textures with ϕ' in range of 30°-80° can be achieved in the sheet by varying the HCE process parameters λ and α. This control of strain and strain path afforded by the HCE enables sheet to be produced under comparable strains, so as to develop similar grain sizes, but with widely different strain paths to achieve varied crystallographic textures. This unique processing characteristic is utilized in the present study to

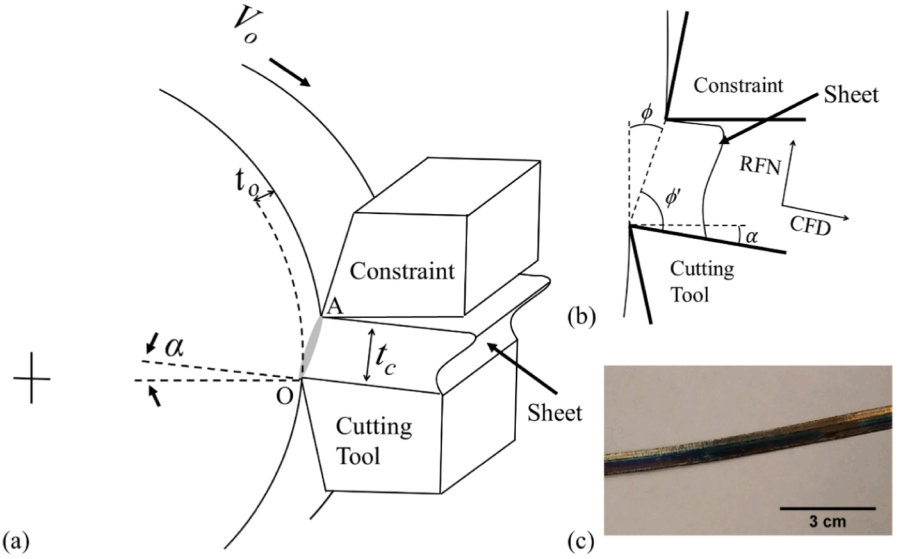

Fig. 1. Shear deformation processing *via* HCE and controllable process parameters. (a) Schematic of rotary HCE process, (b) inset showing a side view of the deformation zone and material flow, and (c) example of sheet produced from Fe-4 wt% Si. Rake face normal (RFN) and chip flow directions (CFD) are marked in the inset.

effectively decouple the influence of texture from that of grain size, thereby enabling study of texture effects on the magnetic properties of the Fe-Si sheet.

Sheet for magnetic properties characterization was produced by HCE from Fe-Si alloy with nominal Si compositions of 4 % and 6.5 % by weight. The 4 % Si workpiece was procured as a commercial hot-rolled plate (Scientific Alloys, Inc.). The detailed composition of the plate was, in wt.%: 3.83Si, 0.028C, 0.018P, 0.015S, 0.006Al, balance Fe. The Fe-6.5 wt% Si alloy was prepared in cylindrical ingot form, in-house, by vacuum induction casting, with high purity Si and interstitial-free steel as charge materials. Representative microstructure images of the two workpieces are shown in Fig. 2. HCE was used to produce sheet with near-constant strains, but with a range of deformation zone orientations (texture), from the two Fe-Si alloys. For the Fe-4 wt% Si alloy, three processing conditions were selected with $\lambda = 1$–2 and $\alpha = 0°$–5°. This corresponded to a near constant strain $\varepsilon = 1.1$–1.4 and texture orientations of $\phi' = 48°$–63°. For the Fe-6.5 wt% Si alloy, a single sheet processing condition ($\lambda = 1$) was explored to isolate the effect of silicon content on magnetic performance. It should be noted here that we are unaware of any Fe-6.5 % Si sheet being produced to date by rolling, especially cold rolling, because of the extremely low cold-workability of this alloy composition. Prior to the magnetic properties' characterization, the sheet samples were given a recrystallization annealing treatment at $T = 700$ °C for 30 min to develop a near-constant equiaxed grain size of $d \sim 25$ μm.

Sheet geometry for each condition are provided in Table 1, along with approximate effective strains imposed during deformation processing. Notably, the initial coarse grain size for both alloy workpieces can lead to heterogenous material flow and microstructure development in the chip/sheet thickness immediately following deformation. However, the severe deformation of HCE paired with post-process heat treatment has been shown to create homogeneous equiaxed microstructures throughout the thickness of annealed Fe-Si sheet, see Fig. 3b and refs. [13,14,18] for additional details. Since the strain imposed in the sheet was approximately the same at the various process conditions, the grain size is expected to be similar in the final sheet products analyzed.

Representative texture and microstructure of a high-silicon content sheet were characterized in the thickness cross-section using optical microscopy and electron backscatter diffraction (EBSD). For optical microstructure analysis, samples were mounted and polished up to a 0.02 μm colloidal silica. Grain structure was revealed using a 5 % Nital solution with mild mechanical agitation. Texture measurement was done using a field-emission scanning electron microscope and EDAX OIM software, with data presented as generated pole figures. Multiple scans were performed on each sample and then merged through the software to provide a large-area view of the texture. EBSD pixel data points were only considered acceptable if a confidence index (CI) of 0.1 or greater was achieved and several hundred pixel data points were sampled from each grain to ensure repeatable orientation mapping. No data cleanup, other than the CI filtering, was employed for generating the pole figures.

Table 1
Summary of the sheet specimen geometries and effective strains imposed during processing.

Sheet Specimen	Chip thickness ratio, λ	Chip thickness, mm	Chip width, mm	Chip length, mm	Effective strain
Fe-4 wt% Si	1	0.1	2.7	102	1.1
	1.5	0.3	3.1	97	1.2
	2	0.2	2.8	100	1.4
Fe-6.5 wt % Si	1	0.1	3.5	100	1.1

Magnetic properties were characterized with the applied field aligned parallel to the length of the HCE-processed Fe-Si sheet using an IEC 60404-4 standard closed-circuit permeameter (Remagraph®C), courtesy of Magnet-Physics, Inc. (Fishers, IN). The annealed sheet samples were clamped within yokes and the polarization (J) was measured using J-compensated coils. Polarization data was converted to induction, B, using $B = \mu_o H + J$, where μ_o is the permeability of vacuum and H is the applied field. Magnetic properties, including maximum permeability (μ_{max}), maximum induction at $H = 60$ kA/m (B_{60}) and coercivity (H_c) were determined from the hysteresis loop measurements. Sheet with a minimum cross-sectional area of 0.3 mm^2 and length of 92 mm were analyzed. For the characterization, the sheet surfaces were prepared by polishing with 600–800 grit SiC abrasive paper, followed by pickling in a 1:5 nitric acid–ethanol solution for 3–5 min to remove any oxides present from the annealing treatment. Hysteresis loops were measured for applied H fields up to ± 60 kA/m at room temperature at a quasi-static rate.

3. Results

Example annealed Fe-Si sheet microstructure and crystallographic texture are shown in Fig. 3a and 3b (see ref. [13]). The sheet texture is expressed by the (0 0 1), (1 0 1) and (1 1 1) pole figures with axes defining the side of the sheet, rake face normal (RFN) and chip flow direction (CFD). The (1 0 1) pole figure is annotated showing two partial inclined {1 1 0} and ⟨1 1 1⟩ fiber texture components indicative of a simple shear texture. The two fibers represent rotations of (1 1 0) crystallographic planes parallel to the shear plane, and an alignment of the ⟨1 1 1⟩ crystallographic direction along the direction of maximum elongation. These fibers are inclined relative to the sheet length (parallel to CFD)

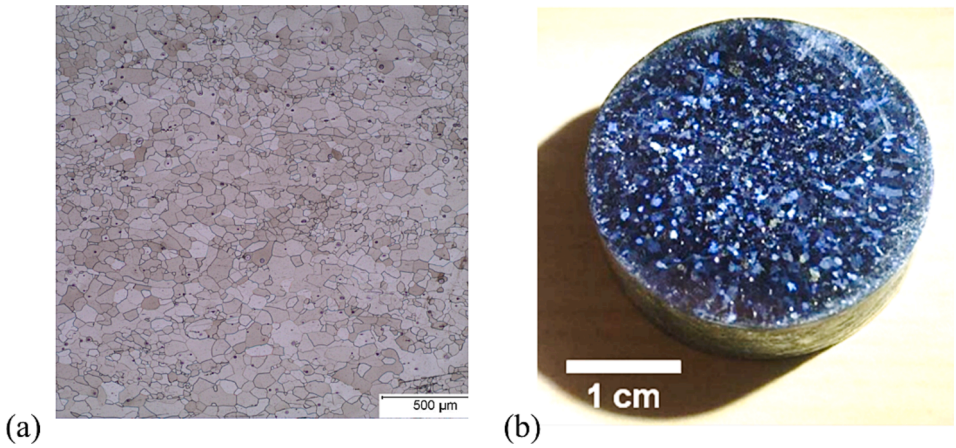

Fig. 2. Initial workpiece microstructures for (a) Fe-4 wt% Si and (b) Fe-6.5 wt% Si.

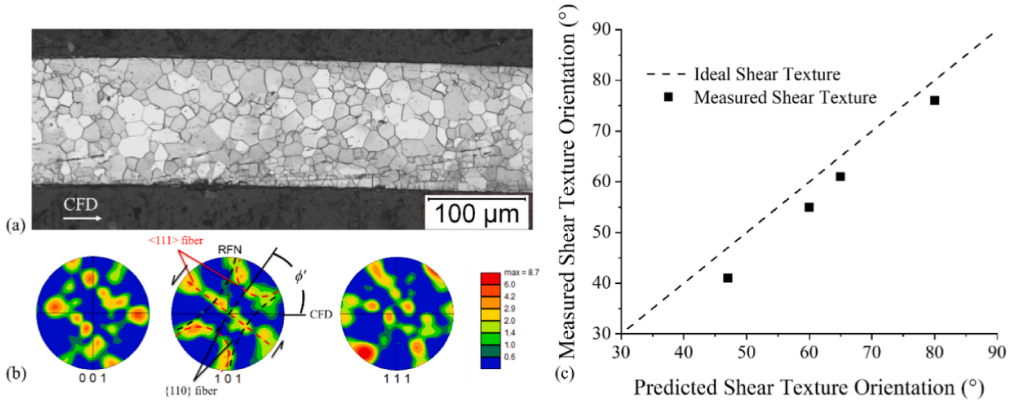

Fig. 3. Microstructure and crystallographic texture in HCE Fe-4 wt% Si sheet. (a) Optical micrograph of microstructure and (b) corresponding (0 0 1), (1 0 1) and (1 1 1) pole figures illustrating the simple-shear texture. Measured shear textures at various deformation conditions are presented in (c) for representative samples and are consistent with the predictions of the shear plane model (Eq. (2)). The latter is plotted as the ideal (shear texture) dashed line.

and can be measured directly on the (1 0 1) pole figure. This type of texture in the strip is referred to as a shear texture [13]. The measured orientations of the shear texture are consistent, to within 5°, with the predictions made using the HCE deformation model and strain path (Eq. (2)), as shown in Fig. 3c (ideal case, dotted line). Note that the measured texture values reported in Fig. 3c were acquired from specimens processed over a wider range of deformation conditions than explored here, i.e., $\phi' = 47°$ to 80°. Similar simple shear textures have also been observed in other single-phase bcc alloys processed by complementary shear-based deformation methods, e.g., equal channel angular extrusion [20–22].

Full-field views of the *B-H* hysteresis loops for the three Fe-4 wt% Si sheet textures and the Fe-6.5 wt% Si sheet are shown in Fig. 4. Corresponding values of maximum permeability, full-field induction (at $H =$ 60 kA/m), and coercivity are tabulated in Table 1. All of specimens show soft magnetic behavior characterized by narrow hysteresis loop widths and high B values at relatively small H fields. Fig. 4a details the hysteresis loop behavior for the Fe-4 wt% Si alloy sheet, with the upper left inset showing a portion of the loops at high H fields encompassing the knee of the magnetization, and the lower right detailing the loops near the graph origin along with the initial magnetization curves. The three loops overlap closely with one another, suggesting that the magnetic performance of the Fe-4 wt% Si sheet is unchanged for the different texture conditions. Data in Table 1 support this observation, with sheet characterized by a narrow range of full-field induction values $B_{60} =$ 1.51–1.61 T, maximum permeability of $\mu_{max} =$ 1441–1783, and coercivity of $H_c =$ 102–124 A/m. Underlying mechanisms for the similarity in the magnetic properties are discussed in Section IV.

Significant differences are however observed between the properties of the 4 wt% Si sheet and the Fe-6.5 wt% Si sheet (Fig. 4b and Table 1). Perhaps the most notable difference is the sharp decrease in the full-field induction and narrower hysteresis loop width for the Fe-6.5 wt% Si alloy sheet ($B_{60} =$ 1.14 T, $H_c =$ 67 A/m) compared to the 4 wt% Si sheet conditions. These differences, coupled with higher maximum permeability of the 6.5 wt% Si alloy ($\mu_{max} =$ 2655), indicate a significantly softer magnetic response for the higher silicon content alloy sheet, an expected effect of the increased Si content [6,23]. Note that while the Fe-6.5 wt% Si is the ideal composition in the Fe-Si binary alloy system for optimizing soft magnetic performance, sheet from this alloy cannot be produced by conventional rolling due to its extremely low (compositionally-driven) workability. In contrast, the HCE is able to produce sheet from this alloy because of the highly confined shear deformation that promotes workability [14]. Notably, sheet were produced without cracks or defects in this study.

4. Discussion

The results have provided insights into the effect of crystallographic texture on magnetic properties in high-Si content Fe alloys, and how these compare with compositional influences.

4.1. Shear texture effects

Despite fundamentally different shear texture orientations for the three Fe-4 wt% Si sheet samples, their magnetic properties did not exhibit any significant differences, with various key property values varying by no more than 20 %. Data in Table 1 suggest that specimens with a smaller texture orientation angle (ϕ') exhibited a slight monotonic decrease in B_{60}, increase in μ_{max}, and decrease in H_c. To assess the role of the ϕ' parameter on the structure-sensitive magnetic properties (μ_{max} and H_c), an analysis was conducted that considers the orientation of the easy ⟨0 0 1⟩ magnetization directions relative to the applied H field along the sheet length. These orientations were used to estimate the change in the crystal anisotropy energy (CAE) for a given processing condition. The CAE provides a quantitative characterization of the resistance to magnetization under an applied H field [2,24,25]. The magnitude of this energy is then a function of the orientation of the easy magnetization directions, and thus of the macroscopic crystallographic texture present in the soft magnetic alloy sheet.

For bcc Fe-Si, a minimum in the CAE occurs when one of the ⟨0 0 1⟩ directions is aligned with the applied flux, leading to softer magnetic performance. A well-known example of this is the commercial grain-oriented (i.e., Goss-textured) Fe-Si rolled sheet in which the microstructure is characterized by a strong {1 1 0} ⟨1 0 0⟩ crystallographic texture, with the ⟨1 0 0⟩ directions aligned with the sheet length. These sheet materials have high permeability and low coercivity when magnetized parallel to the length along the ⟨1 0 0⟩ directions. Magnetization at other orientations leads to comparably harder magnetization performance due to the crystal anisotropy [25]. An estimate of the change in the magnitude of the CAE for a given crystal orientation can be done using the first few terms of the infinite series:

$$CAE = K_0 + K_1(\alpha_1^2\alpha_2^2 + \alpha_2^2\alpha_3^2 + \alpha_3^2\alpha_1^2) + K_2(\alpha_1^2\alpha_2^2\alpha_3^2) + \ldots. \quad (3)$$

where K_0, K_1, K_2 are the anisotropy constants for the material, and the α_n terms are the direction cosines of the three easy magnetization directions relative to the applied field direction [2].

The CAE values computed for our Fe-4 %Si samples are expressed as fractions of the K_o and K_1 for the two simple-shear texture fibers (Fig. 5), while the third term of the series (and beyond) is ignored due to its relatively small contribution [25]. Furthermore, calculation of the CAE

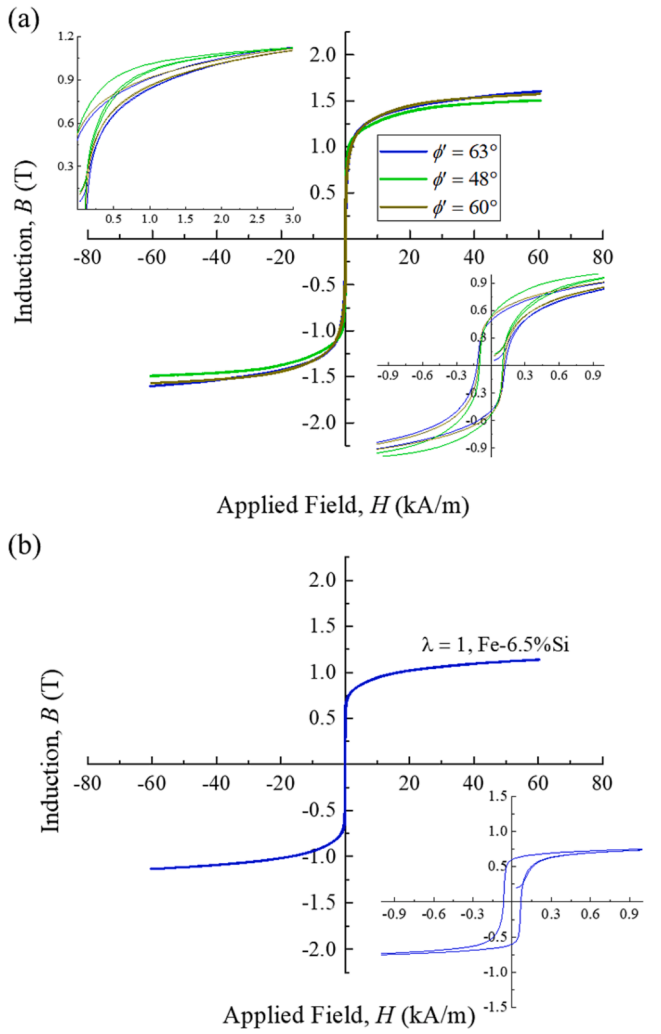

Fig. 4. Hysteresis loops for (a) Fe-4 wt% Si sheet with three different textures and (b) Fe-6.5 wt% Si sheet. For both, the center represents the full-field loops. In (a) the two insets detail a portion of the right quadrant (upper left) and the loops at low-field (lower right). A single inset in (b) shows the loop at low field (lower right). The loops in (a) showed only subtle variation in the magnetic performance for the three different Fe-4 wt% Si sheet texture conditions, suggesting that the shear texture orientation has only a minor effect on the properties. In contrast, significant differences were observed for the Fe-6.5 wt% Si sheets in (b).

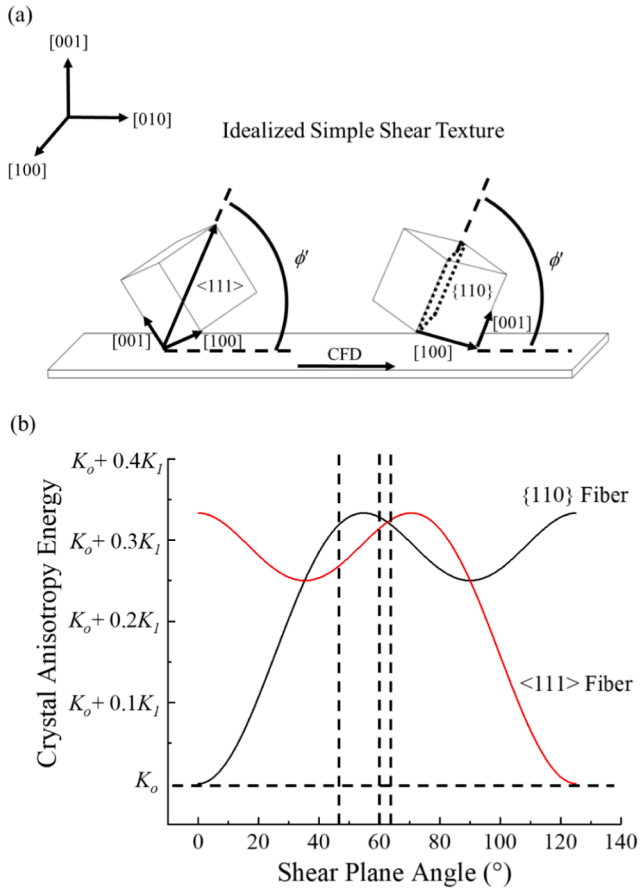

Fig. 5. Crystal anisotropy energy (CAE) and texture. (a) Unit cell representation of the HCE simple-shear texture used to calculate the CAE (see Eq. (3)) for magnetization along the sheet length (chip flow direction). (b) Calculated CAE values for the two positions along the ⟨111⟩ and {110} simple-shear fibers shown in (a) vs shear plane angle (ϕ′). The values of the CAE for the three Fe-4 wt% Si sheet textures (black dotted lines at 48°, 60° and 63°) are compared with trends in the measured magnetic properties.

for the three Fe-4 wt% Si HCE sheet specimens is restricted to considering the shear texture ϕ′ angles for a single position along the two partial simple-shear texture fibers, as illustrated by the unit cell model in Fig. 5a. Superimposed on the model are two of the ⟨001⟩ directions defined by the reference axes in Fig. 5a, with the unit cells inclined at some arbitrary ϕ′ relative to the sheet length. This particular orientation along the two fibers was selected for the CAE analysis due to the symmetry of the [100] and [010] directions about the sheet normal. While this restriction leads to an incomplete description of the full CAE, and thus the full effects of all shear texture components, it nonetheless provides a first-order evaluation for the role of ϕ′. Note that the α_n parameters in Eq. (3) were determined from trigonometric relationships defining the orientations of the three [100], [010], and [001] directions with respect to the H field along the sheet length. The results are shown in Fig. 5b with a plot of the CAE values in terms of K_o and K_1 as a function of ϕ′. Both the {110} (black solid line) and ⟨111⟩ (red solid line) shear texture fibers are shown. The magnitude of the CAE values varied from the angular-independent K_o, at ϕ′ = 0° and 125° for the {110} and ⟨111⟩ fibers, respectively, to local maximums of $K_o + 0.33\,K_1$ at ϕ′ = 55° and 125° for the {110} fiber and ϕ′ = 0° and 70° for the ⟨111⟩ fiber. The CAE for all other orientations ϕ′, which includes the various specimen texture conditions in this study (black dotted lines in Fig. 5b), were found to lie between these extremes.

Insight into the role (or lack thereof) of the shear texture orientation on the μ_{max} and H_c magnetic properties for the three shear-textured Fe-4 wt% Si alloy sheet can be obtained by evaluating these properties with their corresponding CAE values. Fig. 6a shows a plot of the properties and calculated CAE values for the three specimens as a function of ϕ′. The CAE for the ⟨111⟩ fiber (red dotted lined) and {110} fiber (black dotted line) are shown. Properties are shown as solid black points representing the three Fe-4 wt% Si specimens. In terms of identifying a trend in the magnetic properties with the calculated CAE, results were mixed for the two shear texture fibers. CAE for the ⟨111⟩ fiber portion of the texture showed a steady decrease for the three specimens with decreasing ϕ′, while the {110} fiber showed a slight increase for the ϕ′ = 63° and 60° specimen conditions, which decreased again for the ϕ′ = 48° specimen. This is compared to a monotonic increase in the magnetic softness (i.e., increased μ_{max} and decreased H_c) for sheet specimens characterized with decreasing ϕ′. Similar results were also obtained when assessing the role of the shear texture orientation (and CAE) on the permeability of the three specimens over a wide range of H (Fig. 6b). Larger permeability was observed for specimens with a shear texture having a smaller ⟨111⟩ fiber CAE.

From these analyses, it is suggested that the slight increase in

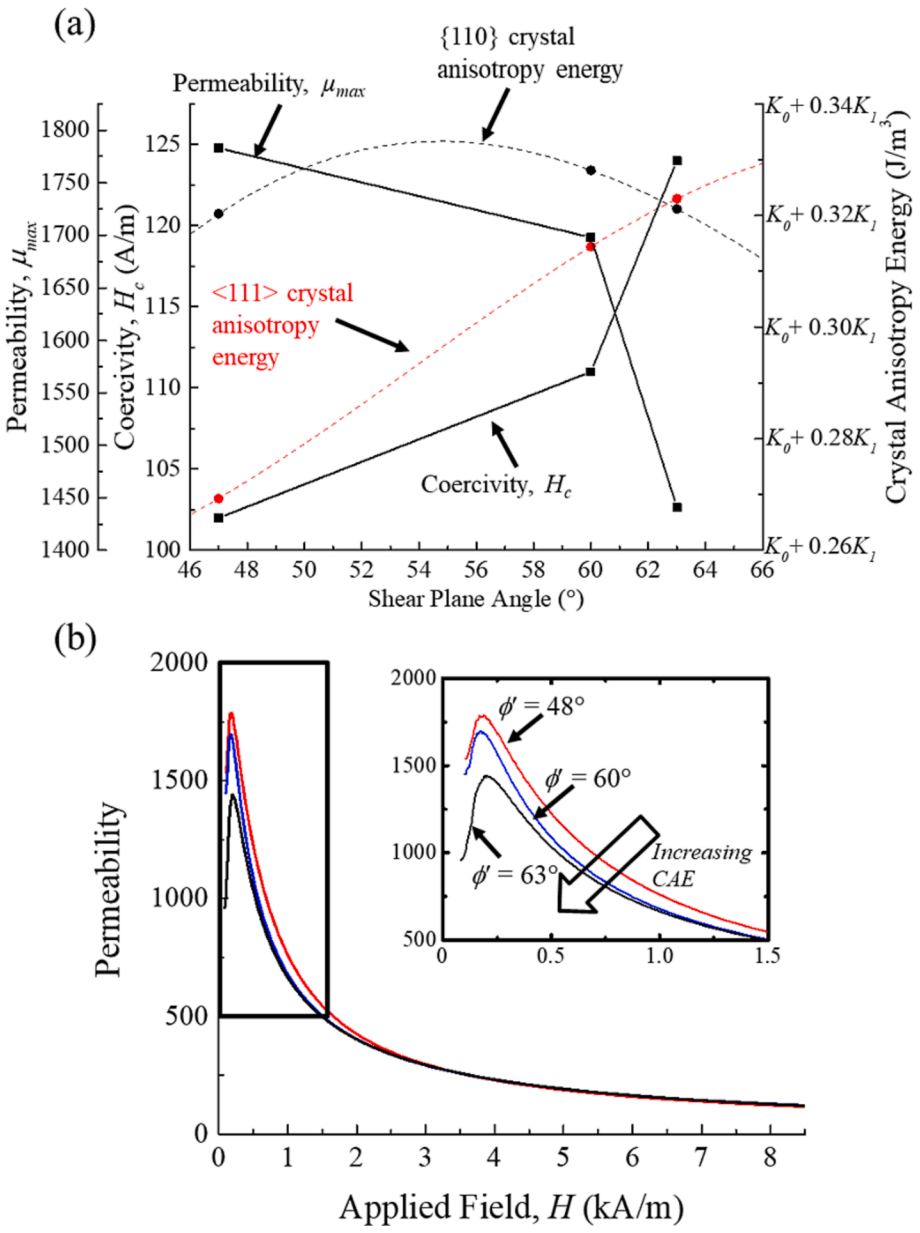

Fig. 6. (a) A plot of the measured permeability and coercivity for the Fe-4 wt% Si sheet with corresponding CAE values calculated for the ⟨1 1 1⟩ and {1 1 0} fibers as a function of the shear plane angle. A slightly increasing permeability and decreasing coercivity is observed with decreasing shear plane angle and CAE, suggested to be the result of a reduced anisotropy energy. This trend was also observed for permeability values over a wide range of H fields (b) approaching saturation.

magnetic softness for specimens with lower ϕ′ may be the result of a favorable change in the orientation of the ⟨1 1 1⟩ crystallographic fiber, leading to a reduction in the corresponding CAE. While it is recognized that the sheet textures are comprised of both ⟨1 1 1⟩ and {1 1 0} fibers, a stronger dependence of the magnetic properties with the ⟨1 1 1⟩ texture fiber is perhaps not surprising since EBSD analysis revealed that this fiber was more pronounced relative to the {1 1 0} fiber (Fig. 3b). Similar descriptions attempting to characterize anisotropic magnetic properties have been demonstrated previously for conventional texture components found in commercial rolled Fe-Si sheet [15,25–28]. Prior investigations have evaluated the role of texture on the magnetic properties of electrical steel sheet, where emphasis is given to the relative orientation of the easy ⟨0 0 1⟩ magnetization crystallographic directions relative to the applied flux direction. Both grain oriented (GO) and non-grain oriented (NGO) electrical steel sheets have been examined. The former is characterized by a notable anisotropy due to the sheet texture in which the ⟨0 0 1⟩ crystallographic directions are aligned with the sheet length/rolling direction. An optimal soft magnetic response is achieved when the magnetic flux is applied along the sheet length. Prior work by Shirkoohi, et al. showed that the hardest magnetic response for GO sheet occurs at approximately 55° relative to the rolling direction, corresponding to the highest CAE [25]. The magnetizing force was observed to increase and the permeability decrease by at least one order-of-magnitude, illustrating a potent impact of the crystallographic texture orientation on the magnetic properties for GO sheet. Investigations on high-Si content electrical steel sheet produced via warm-rolling also illustrate the impact of strong texture components on the magnetic properties. A study by Liang, et al. showed that, through a three-stage warm rolling process, cube textures were developed that increase the magnetic softness in sheet relative to high-Si content sheet produced by the CVD-siliconizing process [27]. Properties improvements included notable reductions in power loss and corresponding increases in magnetic induction for the cube-textured sheet compared to the CVD material.

Relative to GO sheet, NGO sheet are characterized by a significantly weaker crystallographic texture and thus exhibit more isotropic magnetic properties. An investigation by PremKumar, et al. attempted to decouple the role of two textures found in NGO sheet, the ⟨1 0 0⟩- and ⟨1 1 1⟩- fibers oriented parallel to the sheet normal direction, on select magnetic properties [15]. The authors found that a smaller ⟨1 0 0⟩//ND/⟨1 1 1⟩//ND texture intensity ratio enabled improved magnetic performance by reducing power loss and increasing permeability. The texture effects on properties in the study by PremKumar, et al. were significantly smaller than what is observed for GO sheet but were, nonetheless, rationalized as resulting from a corresponding decrease in the total sheet CAE. A study by Xu, et al. on high-Si content NGO electrical steel sheets produced by warm rolling found a similar correlation to improve magnetic properties by limiting the extent of the unfavorable ⟨1 1 1⟩//ND texture fiber component [28]. Overall, magnetic properties of sheet characterized in this study seem only marginally impacted by the orientation of the simple-shear textures that developed in the HCE sheet, similar to previous findings for NGO-type electrical steel sheet produced by conventional rolling processes.

HCE processing conditions will be further explored to optimize the orientation of the ⟨0 0 1⟩ directions and resultant magnetic performance. Emphasis will be placed on exploring deformation conditions that result in a higher shear texture orientation angle during sheet processing, which are predicted to further reduce the CAE contribution for the ⟨1 1 1⟩ -fiber texture component in Fe-Si sheet toward enabling more ideal (softer) magnetic properties (Fig. 5). Higher shear texture orientation angles can be achieved during sheet processing through selection of an adequate chip thickness ratio (λ) and the use of cutting tools with larger positive rake angles (α). Notably, this extent of direct control of the texture orientation for optimizing magnetic performance is not readily achievable in conventional sheet rolling processes.

4.2. Effect of silicon content

A final analysis of the magnetic properties is presented in Table 2 for the HCE-processed Fe-6.5 wt% Si sheet with comparisons to other data from the literature. Note that the literature data represent magnetic properties measurements of Fe-6.5 wt% Si sheet-like material processed by unconventional methods, not rolling. Full-field induction of the HCE Fe-6.5 wt% Si sheet specimen in this study is similar to reported values in other studies, with B_{max} ~ 1.1–1.30 T. Additionally, measured permeability and coercivity values for the HCE-processed Fe-6.5 wt% Si sheet fall within the range of properties reported to date. Literature values encompass a wide range, which are a function of the particular processing route and post-processing heat treatment employed. In general, the softest magnetic performance found to date is from specimens produced by the commercialized CVD-siliconizing process [12,29,30], with large μ_{max} values ranging from 16000 to 58000 and low H_c down to 6 A/m. Other processing routes that produce sheet/ribbon-like specimens show permeability and coercivity properties varying from 2500 to 16400 and 19–150 A/m, respectively [9,31].

While comparison of properties of HCE sheet and those produced by other processing routes are instructive, it should be viewed with caution. Literature data in Table 3 are mostly characteristic of specimens subjected to annealing treatments with time, temperature ranges and highly-controlled reducing environments that are well beyond what are employed in this study; these annealing conditions should promote a comparatively softer magnetic performance for a given alloy composition. Nonetheless, the HCE-processed sheet exhibits structure-sensitive properties that are well within reported ranges of spray-formed versions of the Fe-6.5 wt% Si alloy, and full-field induction properties that are commensurate with alloys produced via other routes. Since an in-depth optimization of post-processing heat treatments, as well as crystallographic texture engineering, was beyond the scope of the present study, a future study will explore opportunities to develop unique annealing textures (e.g., Goss/cube textures) and large grain structures that increase magnetic softness in HCE electrical steel sheet.

Table 2
Summary of the magnetic properties for the the Fe-Si sheet processed by HCE.

Sheet Specimen	Chip thickness ratio, λ	Shear plane angle, ϕ'	Full-field Induction, B_{60} (T)	Maximum Permeability, μ_{max}	Coercivity, H_c (A/m)
Fe-4 wt% Si	1	48	1.51	1783	102
	1.5	60	1.58	1698	111
	2	63	1.61	1441	124
Fe-6.5 wt % Si	1	48	1.14	2655	67

Table 3
Summary of the magnetic properties for the HCE Fe-6.5 wt% Si sheet. Values from other reports for similar high-silicon Fe-Si alloys are also shown for comparison and taken from refs. [9,12,29–31].

Specimen	Full-field Induction, B (T)	Maximum Permeability, μ_{max}	Coercivity, H_c (A/m)
HCE Fe-6.5 wt%Si	1.14	2655	67
PVD Fe-6.5 wt%Si [9]	1.2	16,400	19
Spray formed Fe-6.5 wt%Si [10,31]	–	2500–15270	41–150
CVD Fe-6.5 wt%Si [12,29,30]	1.22–1.30	16000–58000	6

4.3. Implications

With regard to the implications for electromagnetic devices, it is important to consider both the quality of the sheet produced via HCE and the HCE processing itself relative to existing commercial electrical steel sheet products produced by rolling. The quality of high-Si steel sheet, viz., thickness variability and surface roughness, produced by the HCE process is comparable or superior to that of rolled sheet. For sheet, with nominal thickness of 0.5 mm, the thickness variation was within ± 5 % across a sheet width of 21 mm. Fig. 7 shows optical profilometer topographical profiles of the two sides of the sheet. The arithmetic average roughness R_a values are 0.12 ± 0.02 μm and R_a = 0.98 ± 0.11 μm; for reference, the R_a value reported for commercial rolled sheet is typically in the range of 0.4 to 1 μm. Similar trends were observed for the mean peak to valley surfaces roughness, R_z, with values of 0.56 ± 0.04 μm and 4.2 ± 0.87 μm. At least, part of the roughness on one of the faces (back face) of the HCE sheet is due to defect markings from the constraint tool; these can be significantly reduced or even eliminated by better tool grinding. Hence, the HCE sheet, even in its current form, is quite adequate for use in motor core laminations, since its thickness and surface finish are similar to those of rolled strip.

While rolling is a well-established process for high-volume sheet production, the machining-based processing offers some important process advantages also over sheet production by rolling. For example, with regard to process energy, while specific energy data (energy/vol) for sheet production by rolling for high-Si steel strip is not available, energy data for rolled Al and stainless-steel alloy strip are available and can be used to estimate the process energy benefits for the machining-based processing over the rolling. A recent energy analysis has shown that the specific energy for the machining-based processing is ~ 25 % of that for rolling, for Al alloy and stainless steel sheet, for typical industry rolling schedule [32]. The machining-based processing can also produce sheet/foil with thickness down to even 0.05 mm without any cost increase; this is because the strip is produced by a single-step deformation process. In contrast, the cost of rolled strip increases near-exponentially with decrease in section size to foil range due to increase in the number of rolling steps [33]. The smaller thickness sheet/foil enabled by the machining-based processing could be beneficial also for lowering eddy

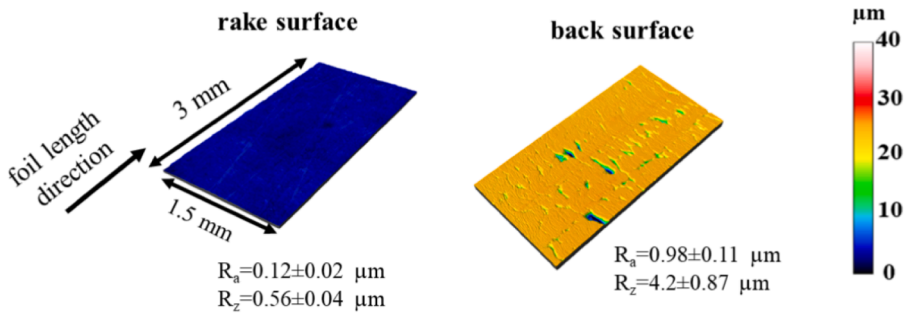

Fig. 7. Representative optical profilometry topographical profiles for high-Si electrical steel sheet produced via HCE. HCE sheet roughness and thickness variation are comparable or superior to rolled sheet.

current losses in motor core lamination applications.

5. Summary

The principal results of the present study pertaining to high-Si content Fe-Si alloys are (1) demonstrating that HCE is a viable thermo-mechanical processing route for producing sheet from these alloys without onset of cracking, unlike typical results from conventional rolling; (2) utilizing the HCE sheet to evaluate crystallographic texture effect (i.e., {1 1 0} and ⟨1 1 1⟩ fiber texture orientations) on magnetic properties of high-silicon content material and concluding that these are minor; and (3) enabling significant improvements in magnetic softness for higher Si-content shear-textured Fe-Si sheet compared to the lower-Si content alloy sheet. Specifically, the Fe-6.5 wt% Si sheet showed an ~ 180 % increase in μ_{max} and a decrease of ~ 240 % in H_c compared to various conditions of the 4 wt% Si alloy sheet. These results also suggest that HCE, with process scaling, can overcome the limitations in conventional rolling to become a viable route for producing Fe-Si sheet for higher-performance electromagnetic devices.

CRediT authorship contribution statement

Andrew B. Kustas: Formal analysis, Investigation, Conceptualization, Methodology, Visualization, Funding acquisition, Writing – original draft, Writing – review & editing. **James B. Mann:** Conceptualization, Funding acquisition, Writing – original draft, Writing – review & editing. **Kevin P. Trumble:** Supervision, Conceptualization, Funding acquisition, Writing – original draft, Writing – review & editing. **Srinivasan Chandrasekar:** Supervision, Conceptualization, Funding acquisition, Writing – original draft, Writing – review & editing.

Declaration of Competing Interest

The authors declare that they have no known competing financial interests or personal relationships that could have appeared to influence the work reported in this paper.

Data availability

Data will be made available on request.

Acknowledgements

The work was supported by the Sandia National Laboratories Laboratory Directed Research & Development (LDRD) office. Additional support for the work at Purdue was provided in part by the U. S. Department of Energy EERE program via Award No. DE-EE0007868 and NSF award CMMI 2100568. Sandia National Laboratories (AK affiliation) is a multi-mission laboratory managed and operated by National Technology and Engineering Solutions of Sandia LLC, a wholly owned subsidiary of Honeywell International Inc. for the U.S. Department of Energy's National Nuclear Security Administration under contract DE-NA0003525. This paper describes objective technical results and analysis. Any subjective views or opinions that might be expressed in the paper do not necessarily represent the views of the U.S. Department of Energy or the United States Government. We would like to also acknowledge the assistance provided by Magnet-Physics, Inc. (Fishers, IN) in measurement of the magnetic properties. This article has been authored by an employee of National Technology & Engineering Solutions of Sandia,LLC under Contract No. DE-NA0003525 with the U.S. Department of Energy (DOE). The employee owns all right, title and interest in and to the article and is solely responsible for its contents. The United States Government retains and the publisher, by accepting the article for publication, acknowledges that the United States Government retains a non-exclusive, paid-up, irrevocable, world-wide license to publish or reproduce the published form of this article or allow others to do so, for United States Government purposes. The DOE will provide public access to these results of federally sponsored research in accordance with the DOE Public Access Plan https://www.energy.gov/downloads/doe-public-access-plan.

References

[1] G. Herzer, Grain Size Dependence of Coercivity and Permeability, IEEE Trans. Magn. 26 (1990) 1397–1402.
[2] B. Cullity, C. Graham, Introduction to magnetic materials, 2011.
[3] C. Chen, Magnetism and Metallurgy of Soft Magnetic Materials, Elsevier North-Holland Inc, New York, N. Y., 1977.
[4] N.P. Goss, New Development in Electrical Strip Steels Characterized by Fine Grain Structure Approaching the Properties of a Single Crystal, Trans. A.S.M. 23 (1935) 511–531.
[5] M.F. Littmann, Iron and Silicon-Iron Alloys, IEEE Trans. Magn. 7 (1970) 48–60.
[6] G. Ouyang, X. Chen, Y. Liang, C. Macziewski, J. Cui, Review of Fe-6.5 wt%Si high silicon steel—A promising soft magnetic material for sub-kHz application, J. Magn. Magn. Mater. 481 (2019) 234–250, https://doi.org/10.1016/j.jmmm.2019.02.089.
[7] C.F. Chang, V. Laxmanan, S.K. Das, Texture and Magnetic Properties of Rapidly Quenched Fe-6.5wt%Si Ribbon, IEEE Trans. Magn. M (1984) 6–11.
[8] H. Fu, Z. Zhang, Y. Jiang, J., Xie, Improvement of magnetic properties of an Fe–6.5wt.% Si alloy by directional solidification, Mater. Lett. 65 (2011) 1416–1419, https://doi.org/10.1016/j.matlet.2011.02.020.
[9] G. Tian, X. Bi, Fabrication and magnetic properties of Fe-6.5% Si alloys by magnetron sputtering method, J. Alloys Compd. 502 (2010) 1–4, https://doi.org/10.1016/j.jallcom.2010.02.175.
[10] C. Bolfarini, M.C.A. Silva, A.M. Jorge, C.S. Kiminami, W.J. Botta, Magnetic properties of spray-formed Fe–6.5%Si and Fe–6.5%Si–1.0%Al after rolling and heat treatment, J. Magn. Magn. Mater. 320 (2008) e653–e656, https://doi.org/10.1016/j.jmmm.2008.04.104.
[11] R. Li, Q. Shen, L. Zhang, T. Zhang, Magnetic properties of high silicon iron sheet fabricated by direct powder rolling, J. Magn. Magn. Mater. 281 (2004) 135–139, https://doi.org/10.1016/j.jmmm.2004.04.098.
[12] H. Haiji, K. Okada, T. Hiratani, M. Abe, M. Ninomiya, Magnetic properties and workability of 6. 5 % Si steel sheet, J. Magn. Magn. Mater. 160 (1996).
[13] A.B. Kustas, D. Sagapuram, K.P. Trumble, S. Chandrasekar, Texture Development in High-Silicon Iron Sheet Produced by Simple Shear Deformation, Metall. Mater. Trans. A Phys. Metall. Mater. Sci. 47 (2016) 3095–3108, https://doi.org/10.1007/s11661-016-3437-3.

[14] A.B. Kustas, D.R. Johnson, K.P. Trumble, S. Chandrasekar, Enhancing workability in sheet production of high silicon content electrical steel through large shear deformation, J. Mater. Process. Technol. 257 (2018) 155–162, https://doi.org/10.1016/j.jmatprotec.2018.02.027.
[15] R. PremKumar, I. Samajdar, N.N. Viswanathan, V. Singal, V. Seshadri, Relative effect(s) of texture and grain size on magnetic properties in a low silicon non-grain oriented electrical steel, J. Magn. Magn. Mater. 264 (2003) 75–85, https://doi.org/10.1016/S0304-8853(03)00142-2.
[16] M. Efe, W. Moscoso, K.P. Trumble, W. Dale Compton, S. Chandrasekar, Mechanics of large strain extrusion machining and application to deformation processing of magnesium alloys, Acta Mater. 60 (2012) 2031–2042, https://doi.org/10.1016/j.actamat.2012.01.018.
[17] D. Sagapuram, M. Efe, W. Moscoso, S. Chandrasekar, K.P. Trumble, Controlling texture in magnesium alloy sheet by shear-based deformation processing, Acta Mater. 61 (2013) 6843–6856, https://doi.org/10.1016/j.actamat.2013.07.063.
[18] A.B. Kustas, D. Sagapuram, S. Chandrasekar, K.P. Trumble, Deformation and recrystallization texture development in Fe-4%Si subjected to large shear deformation, IOP Conf. Ser. Mater. Sci. Eng. (2015), https://doi.org/10.1088/1757-899X/82/1/012054.
[19] Y. Guo, M. Efe, W. Moscoso, D. Sagapuram, K.P. Trumble, S. Chandrasekar, Deformation field in large-strain extrusion machining and implications for deformation processing, Scr. Mater. 66 (2012) 235–238, https://doi.org/10.1016/j.scriptamat.2011.10.045.
[20] I.J. Beyerlein, L.S. Tóth, Texture evolution in equal-channel angular extrusion, Prog. Mater. Sci. 54 (2009) 427–510, https://doi.org/10.1016/j.pmatsci.2009.01.001.
[21] D.F. Susan, T. Jozaghi, I. Karaman, J.M. Rodelas, Equal channel angular extrusion for bulk processing of Fe–Co–2V soft magnetic alloys, part I: Processing and mechanical properties, J. Mater. Res. 33 (2018) 2176–2188, https://doi.org/10.1557/jmr.2018.142.
[22] A.B. Kustas, J.R. Michael, D.F. Susan, I. Karaman, T. Jozaghi, Equal channel angular extrusion for bulk processing of Fe-Co-2V soft magnetic alloys, part II: Texture analysis and magnetic properties, J. Mater. Res. 33 (2018) 2176–2188, https://doi.org/10.1557/jmr.2018.150.
[23] C. Chen, Chih-wen Chen, 1977. https://doi.org/10.1016/B978-0-7204-0706-8.50002-2.
[24] A.D. Rollett, M.L. Storch, E.J. Hilinski, S.R. Goodman, Approach to saturation in textured soft magnetic materials, Metall. Mater. Trans. A Phys. Metall. Mater. Sci. 32 (2001) 2595–2603, https://doi.org/10.1007/s11661-001-0049-2.
[25] G.H. Shirkoohi, M.A.M. Arikat, Anisotropic properties of high permeability grain-oriented 3.25% Si-Fe Electrical Steel, IEEE Trans. Magn. 30 (1994) 928–930, https://doi.org/10.1109/20.312448.
[26] M. Mccarty, G.L. Houze Jr., F.A. Malagari, Texture-Electrical-Property Correlations in Oriented Silicon Steel, J. Appl. Phys. 38 (1967) 1096–1098, https://doi.org/10.1063/1.1709499.
[27] R. Liang, P. Yang, W. Mao, Cube texture evolution and magnetic properties of 6.5 wt% Si electrical steel fabricated by surface energy and three-stage rolling method, J. Magn. Magn. Mater. 457 (2018) 38–45, https://doi.org/10.1016/j.jmmm.2018.02.059.
[28] H.J. Xu, Y.B. Xu, H.T. Jiao, S.F. Cheng, R.D.K. Misra, J.P. Li, Influence of grain size and texture prior to warm rolling on microstructure, texture and magnetic properties of Fe-6.5 wt% Si steel, J. Magn. Magn. Mater. 453 (2018) 236–245, https://doi.org/10.1016/j.jmmm.2018.01.036.
[29] M. Abe, Y. Takada, T. Murakami, Y. Tanaka, Y. Mihara, Magnetic properties of commercially produced Fe-6.5wt% Si sheet, J. Mater. Eng. 11 (1989) 109–116, https://doi.org/10.1007/BF02833761.
[30] Y. Takada, M. Abe, S. Masuda, J. Inagaki, Commercial scale production of Fe-6.5 wt. % Si sheet and its magnetic properties, J. Appl. Phys. 64 (1988) 5367–5369, https://doi.org/10.1063/1.342373.
[31] C.C. Lima, M.C.A. da Silva, M.D.C. Sobral, R.E. Coelho, C. Bolfarini, Effects of order–disorder reactions on rapidly quenched Fe–6.5%Si alloy, J. Alloys Compd. 586 (2014) S314–S316, https://doi.org/10.1016/j.jallcom.2012.09.074.
[32] S. Chandrasekar, K.P. Trumble, J.B. Mann, A. Rohatgi, M. Efe, High-Silicon steel strip by single-step shear deformation processing Final Report for DOE EERE-AMO Award DE-EE0007868, 2022.
[33] F.H. Froes, M.N. Gungor, M.A. Imam, Cost-affordable titanium: The component fabrication perspective, JOM 59 (2007) 28–31, https://doi.org/10.1007/s11837-007-0074-8.